ACS Photonics

Letter

Cite This: ACS Photonics 2019, 6, 1365−1371

pubs.acs.org/journal/apchd5

Second Harmonic Generation from Phononic Epsilon-Near-Zero Berreman Modes in Ultrathin Polar Crystal Films

Nikolai Christian Passler,*[,†] I. Razdolski,[†] D. Scott Katzer,[‡] D. F. Storm,[‡] Joshua D. Caldwell,[‡,§] Martin Wolf,[†] and Alexander Paarmann*[,†]

[†]Fritz-Haber-Institut der Max-Planck-Gesellschaft, Faradayweg 4-6, 14195 Berlin, Germany

[‡]U.S. Naval Research Laboratory, 4555 Overlook Avenue SW, Washington, D.C. 20375, United States

[§]Vanderbilt University, Institute of Nanoscale Science and Engineering, 2201 West End Avenue, PMB 350106, Nashville, Tennessee 37235-0106, United States

Supporting Information

ABSTRACT: Immense optical field enhancement was predicted to occur for the Berreman mode in ultrathin films at frequencies in the vicinity of epsilon-near-zero (ENZ). Here, we report the first experimental proof of this prediction in the mid-infrared by probing the resonantly enhanced second harmonic generation (SHG) at the longitudinal optic phonon frequency from a deeply subwavelength-thin aluminum nitride (AlN) film. Employing a transfer matrix formalism, we show that the field enhancement is completely localized inside the AlN layer, revealing that the observed SHG signal of the Berreman mode is solely generated in the AlN film. Our results demonstrate that ENZ Berreman modes in intrinsically low-loss polar dielectric crystals constitute a promising platform for nonlinear nanophotonic applications.

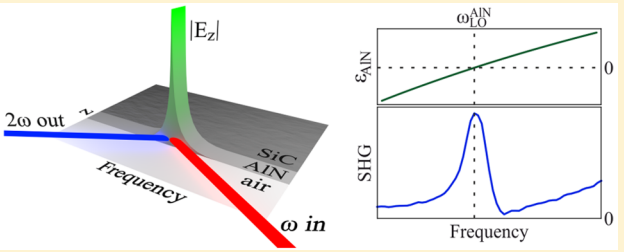

KEYWORDS: *Berreman mode, epsilon-near-zero, infrared, nanophotonics, second harmonic generation, field enhancement*

In nanophotonics, nonlinear optical phenomena are driven by the enhancement of local optical fields, which arises due to polaritonic resonances. These are traditionally observed as plasmon polaritons in metallic nanostructures or rough metal surfaces. Such strongly enhanced fields enable a variety of nanoscale applications,[1] such as all-optical switching,[2,3] low-loss frequency conversion,[4,5] and highly efficient sensing.[6,7] In the infrared (IR), an alternative to plasmonic resonances in metals are phonon polaritons supported in polar crystals,[8] as has been demonstrated in various seminal studies.[9−12] These phonon polaritons feature longer lifetimes than plasmon polaritons, leading to much larger quality factors and stronger field enhancements,[13−15] and thus, potentially enhanced efficiency of nonlinear optical effects.

One area in nanophotonics of distinct recent interest are investigations of polaritonic modes in plasmonic or polar dielectric subwavelength-thin films that emerge near zero permittivity. Over the past decades, the existence of such thin-film polaritonic modes has attracted broad attention.[16−26] Initially, radiation in a narrow spectral window at the plasma frequency of thin metal films was predicted[16] and later observed.[18−20] Its origin was associated with a collective surface plasma mode with polarization normal to the surface plane of the film.[18] At the same time, a similar effect was reported by Berreman in a thin polar dielectric film,[17] where absorption occurs at the longitudinal optic (LO) phonon frequency.

These absorption features in thin films were argued to originate in radiative virtual polaritonic modes,[21,22,24] naturally occurring at frequencies where the real part of the dielectric function crosses zero. This condition is met at the plasma frequency in a metal, and at the LO frequency of a polar crystal film. While these lossy polariton modes disperse on the low momentum side of the light line, it was discovered that a complementary evanescent polariton mode close to the LO frequency of a polar dielectric is also supported outside the light cone.[22] Just like the radiative modes, the evanescent polaritons naturally emerge in thin films at frequencies of vanishing dielectric function. Therefore, these modes offer an intriguing platform for exploiting the unique characteristics of waves propagating in so-called epsilon-near-zero (ENZ) materials.[27,28]

While most ENZ studies depend on carefully and intricately designed metamaterials,[29−32] thin metal or polar dielectric films stand out for their structural simplicity. Previous studies have reported promising applications employing these ENZ polariton modes, such as optoelectronic devices for the ultrafast control of absorption and emissivity,[33−35] directionally perfect absorption,[36,37] or long-range plasmon polaritons for the development of nanophotonic integrated technologies.[38,39]

Received: February 20, 2019
Published: June 3, 2019

DOI: 10.1021/acsphotonics.9b00290
ACS Photonics 2019, 6, 1365−1371

However, these previous studies mostly focused on the linear optical response, whereas only few reports of the nonlinear conversion efficiency of ultrathin films exist. This efficiency has been proposed to be strongly enhanced at ENZ frequencies,[40] but experimental verification is limited to a few studies of indium tin oxide (ITO) thin layers[41−43] excited at frequencies in the near-infrared spectral range. The nonlinear optical response of thin films of other materials with phonon resonances in the mid- to far-IR, in particular III−V or III-nitride polar semiconductor compounds, however, has to the best of our knowledge not yet been studied.

In this work, we investigate the linear and nonlinear optical response of ultrathin ($\lambda/1000$) AlN films on a SiC substrate in the radiative regime, where λ represents the free-space wavelength at the ENZ condition. We report strong SHG at the AlN LO phonon frequency arising from the Berreman mode in the ultrathin AlN film. The observed SHG yield provides experimental proof of the immense field enhancement inside the film and is attributed to the excitation of the Berreman resonance. Furthermore, we delineate several perspectives based on ENZ polaritons for the deployment of low-loss nonlinear nanophotonic applications.

A mode in a medium is defined as a solution of Maxwell's equations in the absence of an external perturbation. In a three-layer system, the dispersion of a polaritonic mode can be calculated by numerical evaluation of the following formula:[20,25,44]

$$1 + \frac{\varepsilon_1 k_{z3}}{\varepsilon_3 k_{z1}} = i \tan(k_{z2} d)\left(\frac{\varepsilon_2 k_{z3}}{\varepsilon_3 k_{z2}} + \frac{\varepsilon_1 k_{z2}}{\varepsilon_2 k_{z1}}\right) \quad (1)$$

where ε is the dielectric function, d is the film thickness of layer 2, $k_{zi} = \sqrt{\frac{\omega^2}{c^2}\varepsilon_i - k_x^2}$ is the out-of-plane momentum, k_x is the in-plane momentum conserved in all layers, and the subscripts i = 1, 2, and 3 refer to the three layered media. In principle, eq 1 can be solved either for a complex frequency ω and a real wavevector k_x, or for a complex k_x and a real ω. However, depending on the mode nature and the observables of interest, one of the representations is better suited than the other. We here choose the complex ω representation, following the rationales found in literature,[25,33,45,46] especially to account for the virtual nature of the Berreman mode[47] (for further details, see Supporting Information, Figure S1).

By solving eq 1 for an air/AlN/air system with varying thickness d_{AlN} of the AlN layer, the dispersion curves shown in Figure 1a are obtained. On the right-hand side of the light line, that is, in the region of evanescent surface-bound solutions, the symmetric (upper blue lines) and antisymmetric (lower blue lines) thin-film polaritons emerge. Spectrally, these modes are bound inside the AlN reststrahlen region between the TO and LO frequencies ω_{TO}^{AlN} and ω_{LO}^{AlN}, respectively. For thick films ($d_{AlN} > 1$), the two modes enclose the dispersion of a surface phonon polariton (SPhP) at the interface of a bulk AlN crystal (green line) and, for further increasing film thicknesses, eventually fall back onto this single green curve. On the other hand, for diminishing thicknesses, the two modes are pushed toward ω_{TO}^{AlN} and ω_{LO}^{AlN}. For d_{AlN} = 20 (solid line), the upper mode features a flat dispersion curve in the vicinity of ω_{LO}^{AlN}. At this frequency, the dielectric function approaches zero, and hence, the upper mode is an ENZ thin-film polariton.

The Berreman mode (red lines) arises as a continuation on the left-hand side of the light line, that is, in the region of

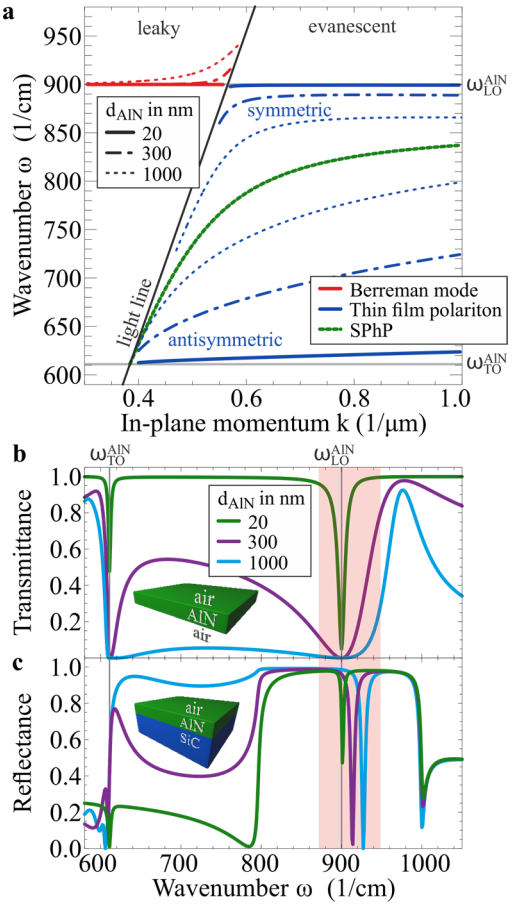

Figure 1. Berreman mode in a freestanding AlN film and on a SiC substrate. (a) Calculated dispersions of the Berreman mode and thin film polaritons in a freestanding AlN film, and that of a SPhP at the surface of a bulk AlN crystal. The Berreman mode is flat (red line) for ultrathin films ($d < \lambda/500$), while thicker films (dash dotted/dotted red lines) result in a dispersion bending upward in the vicinity of the light line in vacuum (black line). Analogous to the symmetric thin film polariton (blue line, upper branch), the dispersion of the Berreman mode lies close to the LO frequency where the real part of the dielectric function exhibits a zero-crossing. (b) Calculated transmittance of a freestanding AlN thin film for three different film thicknesses d_{AlN} at an incidence angle of 85°. The dip at the LO frequency for the thinnest film corresponds to the Berreman mode (red shade), which disappears with the buildup of the AlN reststrahlen band for increasing film thicknesses. (c) Calculated reflectance of an AlN thin film on a SiC substrate at an incidence angle of 85°. Here, the Berreman mode appears as a deep dip inside the reststrahlen band of SiC.

radiative solutions. Contrary to its evanescent counterpart, this leaky polariton mode undergoes a small upward bend close to the light line for larger film thicknesses. For d_{AlN} = 20 nm, however, the Berreman mode has a flat dispersion at ω_{LO} just like the evanescent polariton and, therefore, also exhibits ENZ character.

The feature in the transmittance spectrum of a thin film at the LO frequency originally reported by Berreman[17] is reproduced in the transmittance simulations shown in Figure 1b. The Berreman mode can only be excited by radiation with a nonzero out-of-plane electric field component, and hence p-polarized light at oblique incidence is required to observe the absorption peak. A visual explanation for the necessity of p-polarized excitation can be found in the spatial electric field

DOI: 10.1021/acsphotonics.9b00290
ACS Photonics 2019, 6, 1365−1371

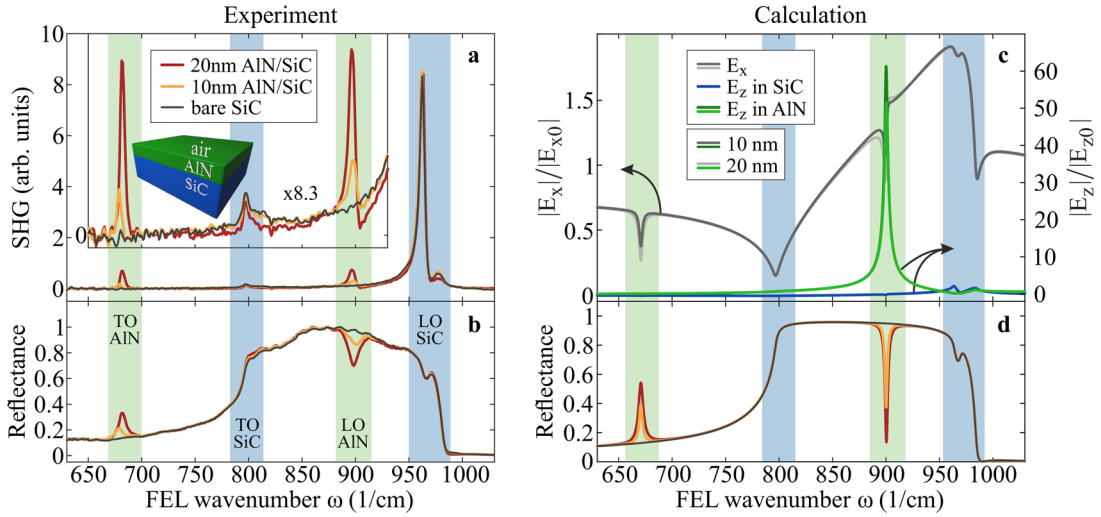

Figure 2. Strongly enhanced SHG from a Berreman mode in AlN. (a, b) Experimental SHG and reflectance spectra, respectively, taken for three samples consisting of (i) a 20 nm, (ii) a 10 nm thin AlN film on a 4H-SiC substrate, and (iii) a bare 4H-SiC crystal. Compared to the reference sample (iii), the AlN thin films only differ at the TO and LO frequencies of AlN, exhibiting small features in the reflectance and a strong SHG signal (enlarged by a factor of 8.3 in the inset in a). The origin of the strong SHG yield is illustrated in (c). While the in-plane E_x field enhancement is small at the AlN/SiC interface (gray lines, left y-axis), the out-of-plane E_z fields feature a strong enhancement of >60 at the AlN LO frequency (green lines, right y-axis). On the SiC side of the AlN/SiC interface, the E_z fields are small (blue line), revealing that the field enhancement is strictly confined inside the nanometric AlN layer. (d) Calculated reflectance curves of the investigated samples, being in excellent agreement with the experiment.

distribution of the Berreman mode (see Supporting Information and Figure 2a,b). Along the in-plane coordinate x, the field vectors perform a rotation in the x-z plane, that is, the plane of incidence, with z being the out-of-plane coordinate. In order to accentuate the Berreman absorption feature, the curves shown in Figure 1b and c were calculated at an incidence angle of 85°, leading to a strongly pronounced dip at ω_{LO}^{AlN} = 900 for d_{AlN} = 20 nm.

The transition from an ultrathin AlN film with d_{AlN} = 20 nm to a thicker one with d_{AlN} = 1000 nm, is characterized by the buildup of the AlN reststrahlen band, featuring vanishing transmittance between the TO and LO frequencies, as shown in Figure 1b. Because of this buildup, already for d_{AlN} = 300 nm, the Berreman absorption dip is strongly broadened and its frequency position is not clearly defined. This is different in Figure 1c, were we show the reflectance curves for an air/AlN/SiC structure, resembling the experimentally investigated sample. Interestingly, the highly reflective reststrahlen band of the SiC substrate allows to observe the Berreman absorption feature in a reflectance measurement. In contrast to the freestanding film, a sharp and deep minimum is observed even for 1000 nm film thickness, indicating that the Berreman mode is still supported at the thick-film limit. In the Supporting Information, Figure S3b, the reflectance is shown for film thicknesses up to 5 μm. For d_{AlN} > 1.5 μm, the amplitude of the Berreman dip starts to diminish, approaching the optical response of a bulk AlN crystal that does not support a Berreman mode anymore.

In order to verify that the reflectance dips in Figure 1c originate in the Berreman mode, the theoretical dispersion for the air/AlN/SiC structure is calculated employing eq 1. While being quantitatively similar to the air/AlN/air Berreman mode dispersion, the SiC substrate leads to a smaller slope and a reduced frequency in proximity to the light line (see Supporting Information, Figure S3a). As is shown in Supporting Information, Figure S3b, the frequencies of the theoretical dispersion at 85° incidence angle and those of the numerical reflectance curves are in excellent agreement, corroborating that a reflectance measurement gives experimental access to the Berreman mode of the air/AlN/SiC structure.

We employ SHG spectroscopy[48] to probe the field enhancement associated with the excitation of the Berreman mode. The strongest field confinement occurs in ultrathin films leading to a strong field enhancement of the Berreman mode, which is a prerequisite for the observation of a significant SHG signal. We therefore focus on two samples with ultrathin AlN films of thickness d_{AlN} = 10 and 20 nm. The AlN films were grown by RF-plasma assisted molecular beam epitaxy onto a 4H-SiC substrate and, therefore, also feature a hexagonal crystal structure with the c-axis being perpendicular to the sample surface.

The reflectance and SHG spectroscopy measurements were performed in a noncollinear autocorrelator setup[48] at 30° and 60° incidence angle employing a tunable, narrow-band, p-polarized mid-IR free electron laser (FEL)[49] as an excitation source. Beforehand, intrinsic higher harmonics of the FEL are blocked by two dichroic 7 μm long-pass filters. The reflectance is recorded at 60° by a pyroelectric detector, whereas the two-pulse correlated SHG signal is generated at 45° between the reflected fundamental beams and is measured by a mercury–cadmium–telluride detector. For two p-polarized incident beams, the produced SHG signal is also p-polarized (PPP configuration). Because of the respective $\chi^{(2)}$ component for c-cut crystals being zero, there is no SPP contribution.[48,50] We note that the noncollinear excitation scheme is only applicable for ultrathin films where the shift of the Berreman resonance frequency with incidence angle is negligible (see Figure 1a), whereas for thicker films, a collinear setup would be necessary.[51]

The experimental SHG and reflectance spectra are plotted in Figure 2a and b, respectively. There, the yellow and red lines

DOI: 10.1021/acsphotonics.9b00290
ACS Photonics 2019, 6, 1365−1371

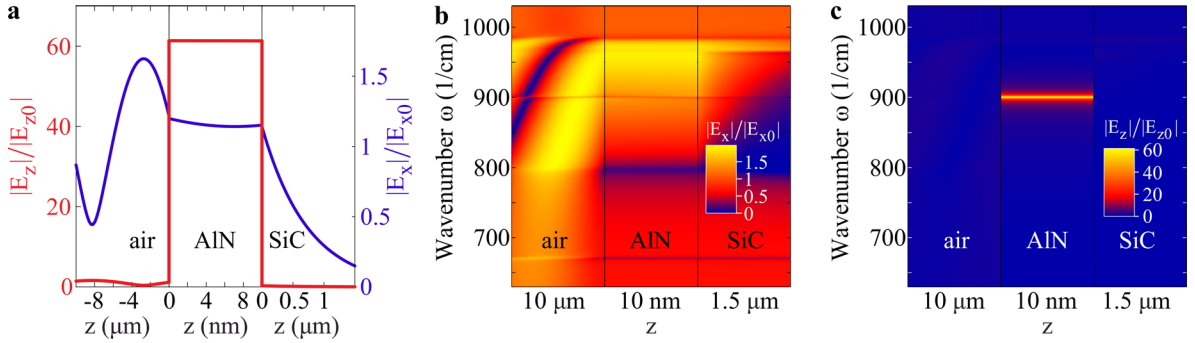

Figure 3. Field enhancement in a 10 nm thin AlN film. (a) In-plane and out-of-plane normalized fields E_x and E_z, respectively, along the z axis perpendicular to the interfaces and calculated at the Berreman resonance at 900 cm^{-1}. The large E_z field enhancement (red) is strongly localized inside the AlN. The E_x field (blue), on the other hand, does not feature any significant field enhancement. Note that in the air layer, the sum of the normalized incoming wave and the reflected wave is plotted, thus resulting in amplitudes larger than 1. (b, c) Spatio-spectral maps of E_x and E_z, respectively. The in-plane field E_x features a small enhancement at the SiC LO (965 cm^{-1}) and a minimum at the SiC TO (797 cm^{-1}). In between in the SiC reststrahlen band, the field decays evanescently into the SiC substrate. Interestingly, a local minimum in E_x can be observed at both the AlN TO (670 cm^{-1}) and the AlN LO (900 cm^{-1}). On the contrary, the out-of-plane field E_z in (c) features an immense and spectrally sharp field enhancement inside the AlN layer at the AlN LO frequency.

indicate the data for the 10 and 20 nm thick AlN films, respectively. Additionally, we show spectra for a bare SiC sample (black lines). As has been demonstrated previously,[48,50] the bulk SiC substrate produces SHG peaks at its TO and LO frequencies (blue shades), leading to the same response in all three samples in these regions ($\omega \sim 800$ and 970 cm^{-1}). In fact, the only deviations from the bulk reflectance and SHG spectra are seen at the AlN TO and LO frequencies (green shades), where we observe clear, strong peaks in the SHG signal scaling with the AlN film thickness (see inset in Figure 2a with enlarged vertical axis). The observation of such a sizable SHG yield at the LO frequency is astonishing, especially considering the exceptionally small effective volume of only a few nanometer AlN that is generating the signal.

The SHG intensity I_{SHG} is proportional to the tensor product of the field enhancement $\vec{E}(\omega)$ and the second-order susceptibility tensor $\chi^{(2)}$:[52]

$$I_{SHG} \propto \left|\chi^{(2)}(-2\omega;\ \omega,\ \omega)\vec{E}(\omega)\vec{E}(\omega)\right|^2 \tag{2}$$

It is clear that either a resonance peak in $\chi^{(2)}$ or $\vec{E}(\omega)$ will lead to an enhanced SHG yield and thus a peak in the SHG spectrum. However, at the LO frequency, the second-order susceptibility $\chi^{(2)}$ has no resonances.[48] As for the case of polaritons,[51] also here we do not need to introduce an additional resonance in the $\chi^{(2)}$ to reproduce the data. We therefore argue that the origin of the reported large SHG yield is the immense electric field enhancement in the AlN thin film. In order to get further insights into the electric field distributions, we employ a 4 × 4 transfer matrix formalism specifically designed to simultaneously handle media with fully anisotropic as well as isotropic dielectric tensors.[53] This allows us to account for the uniaxial anisotropy of both 4H-SiC and hexagonal AlN, leading to an accurate reproduction of the reflectance data with highly detailed qualitative accordance. For instance, even small features like the dip at the high-frequency reststrahlen edge of SiC originating from the SiC anisotropy are accurately reproduced, see Figure 2d. (Note that for Figure 1 the materials were taken to be isotropic, which is sufficient for the qualitative understanding of the Berreman mode.)

Quantitatively, the calculations feature a deeper and sharper Berreman dip in the reflectance than in the experiments, see Figure 2b. This discrepancy is mainly due to growth defects in the AlN layer and an unavoidable strain due to the lattice mismatch between SiC and AlN (1%),[54,55] leading to an effectively increased damping constant of AlN than assumed in the calculations (γ_{AlN} = 2.2 cm^{-1}).[56] Furthermore, an additional experimental broadening arises from the FEL line width (~4 cm^{-1}).

In Figure 2c, we show the in-plane (E_x) and out-of-plane (E_z) local electric field enhancements at the AlN/SiC interface in both media. Note that E_x and E_z are normalized to their respective incoming field amplitudes E_{x0} and E_{z0}. While E_x is conserved at the interface and is generally small (with a maximum value of ~1.9), the E_z field enhancement features a strong peak at ω_{LO}^{AlN} with a maximum of >60 for the 10 nm film.

Note that while the Berreman reflectance minimum deepens for larger film thicknesses, the E_z field enhancement is already 16% smaller in the 20 nm than in the 10 nm film. Thus, counterintuitively, thicker films that feature higher optical absorption, exhibit a smaller degree of field enhancement. In the observed SHG signal, this reduction is compensated by an increasing effective volume, leading to larger SHG yields. However, we emphasize that only ultrathin films (d_{AlN} < 50 nm) demonstrate such high field intensities, thus, opening new possibilities for deeply subwavelength nanophotonic applications in the IR.

The E_z field is fully confined inside the AlN layer, which is reflected in the flat frequency dependence and small magnitude of the E_z field enhancement in SiC (blue line in Figure 2c). This field localization is even better illustrated in Figure 3a, where we show the spatial distribution of the in-plane E_x and out-of-plane E_z field enhancements as a function of z, that is, along the surface normal, at ω = 900 cm^{-1}. The electric field has to obey Maxwell's boundary conditions, that is, continuity of the in-plane fields ($E_x^{air} = E_x^{AlN}$ and $E_y^{air} = E_y^{AlN}$) and of the out-of-plane displacement field $D_z = \varepsilon E_z$ is required:

$$\varepsilon_{air}E_z^{air} = \varepsilon_{AlN}E_z^{AlN} \tag{3}$$

Equation 3 is the physical reason for a field enhancement at ENZ conditions, since for vanishing ε_{AlN} adjacent to air with a finite ε_{air}, the electric field E_z^{AlN} strongly increases in order to

DOI: 10.1021/acsphotonics.9b00290
ACS Photonics 2019, 6, 1365−1371

fulfill the boundary condition. In a bulk crystal, the field enhancement at ENZ conditions typically reaches values on the order of 1−10 (e.g., in bare SiC[48] or in an AlN/SiC structure, see Supporting Information, Figure S4a).

However, in a bulk crystal the phase difference of the incoming and the reflected fields is close to zero, leading to a small total field at the air/AlN interface (E_z^{air}) due to destructive interference. As a consequence, following eq 3, the ENZ induced enhancement of the E_z^{AlN} field is strongly suppressed. In contrast, in the limit of an ultrathin AlN film ($d_{\mathrm{AlN}} \lesssim 100$ nm), the phase difference becomes sizable, thus, leading to the strong field enhancement as shown in Figure 2c and Figure 3a (for details, see Supporting Information, Figure S4b−g).

Figure 3b and c show spatio-spectral maps of the E_x and E_z fields each normalized to E_{x0} and E_{z0}, respectively. Interestingly, E_x features no considerable field enhancement, but exhibits small dips or peaks marking the TO and LO frequencies of both AlN and SiC. The spatio-spectral map of E_z in Figure 3c, on the other hand, clearly reveals the extreme, spectrally sharp and strongly confined field enhancement in the AlN layer at $\omega = 900\ \mathrm{cm}^{-1}$.

Finally, we turn to the TO frequency of AlN (670 cm^{-1}),[57] where the experimental data in Figure 2a exhibit a strong SHG signal of similar magnitude as at the LO frequency. Quite surprisingly, this AlN TO peak is even larger than the peak at the TO frequency of the SiC substrate. Partially, this can be attributed to a reduced field suppression at ω_{TO} for thin films compared to a bulk crystal[52] (see Supporting Information, Figure S5). Notably, the observed peak arises from a resonance in the second-order susceptibility $\chi^{(2)}$ at $\omega_{\mathrm{TO}}^{\mathrm{AlN}}$, and not from a field enhancement as for the LO peak. Therefore, to fully understand the SHG peak amplitudes at the TO frequencies, a quantitative model of the $\chi^{(2)}$ for AlN would be necessary.

In this work, we have observed an immense SHG signal arising from a Berreman mode in an ultrathin AlN film excited at ENZ frequencies in the mid-IR. Analogous to previous studies of ITO,[58] aluminum-doped ZnO,[59] and CdO,[60] the high optical nonlinearity at ENZ conditions in our system holds high promises for all-optical ultrafast control of polarization switching,[60] and even over the material's optical properties.[58,59] However, while all mentioned studies employ ultrathin films excited via free-space radiation, for which in our system the Berreman mode is accessible, dispersing inside the light cone in vacuum, a complementary polaritonic ENZ mode exists on the other side of the light line. The linear response of these ENZ polaritons has been studied recently,[61,62] but investigations of their nonlinear response are to the best of our knowledge still lacking. Analogous to the Berreman mode, a strong field enhancement also characterizes the ENZ thin film polariton due to its ENZ environment. We, therefore, highlight the nonlinear response of ENZ polaritons to be an intriguing subject, specifically in light of the development of polariton-based nonlinear nanophotonics.

Polar crystals such as AlN or SiC, where ENZ conditions are met at the LO phonon resonances in the mid-IR, feature several appealing properties that are unavailable in metals or ITO: (i) The imaginary part of the dielectric function ε_2 at ω_{LO} ($\varepsilon_{\mathrm{AlN}}(\omega = \omega_{\mathrm{LO}}) = 0 + 0.02i$) is significantly smaller than in metals,[63] and more than 1 order of magnitude smaller than for ITO ($\varepsilon_{\mathrm{ITO}}(\omega = \omega_{\mathrm{LO}}) = 0 + 0.5i$),[43] which strongly increases the field enhancement inside the thin layer and, hence, the SHG efficiency. (ii) Many polytypes of SiC as well as AlN exhibit a hexagonal crystal structure, resulting in a uniaxial anisotropy of the dielectric tensor. This anisotropy leads to a hyperbolic frequency region between the extraordinary and ordinary LO frequencies, that is, in the range of the ENZ polaritons, enabling a whole new range of phenomena yet to be explored. These phenomena include, as has been observed in different systems before, negative refraction,[64] negative phase velocity,[65] or subdiffraction imaging and focusing.[66,67] (iii) Compared to highly doped semiconductors, one drawback of polar crystals is the lack of tunability of the ENZ frequency, being fixed to the LO phonon. On the other hand, due to relatively short lifetimes of surface plasmon polaritons in metals or most highly doped semiconductors, plasmon-based nanophotonics exhibits intrinsic drawbacks due to inherently high losses, whereas SPhPs in polar crystals feature much longer polariton lifetimes due to long-lived phonon resonances.[8,68] Hence, the employment of the ENZ polariton at the LO frequency offers an appealing alternative for nanophotonic applications, where low-loss ENZ characteristics combine with ultrahigh field enhancements.

In conclusion, we have reported the first observation of a resonantly enhanced SHG yield from a phononic Berreman mode in a deeply subwavelength thin film, exemplified for AlN on a 4H-SiC substrate. The origin of this large SHG signal is the immense out-of-plane field enhancement arising due to the zero-crossing of the dielectric function at the thin film LO frequency, strongly confined to the ultrathin layer. Thanks to low phonon dampings in polar crystals such as AlN and SiC, nanophotonic systems based on such crystals offer an appealing alternative to plasmonics, featuring high-quality resonances with extreme field enhancements. As a possible pathway, we envision ultrathin-film Berreman modes featuring ENZ nature to provide new opportunities for ultrafast all-optical control by taking advantage of the high optical nonlinearity.

■ ASSOCIATED CONTENT

Supporting Information

The Supporting Information is available free of charge on the ACS Publications website at DOI: 10.1021/acsphotonics.9b00290.

Theoretical thin film polariton dispersions for either complex frequency or in-plane momentum (Figure S1); Electric field distribution of the Berreman mode in a 1 μm thick AlN slab (Figure S2); Comparsion of theoretically and numerically determined Berreman dispersion (Figure S3); Out-of-plane field enhancement E_z at the interfaces of the air/AlN/SiC system (Figure S4); Contributions to the SHG yield at the AlN TO frequency (Figure S5) (PDF)

■ AUTHOR INFORMATION

Corresponding Authors

*E-mail: passler@fhi-berlin.mpg.de.
*E-mail: alexander.paarmann@fhi-berlin.mpg.de.

ORCID

Nikolai Christian Passler: 0000-0002-7477-8611
Joshua D. Caldwell: 0000-0003-0374-2168
Alexander Paarmann: 0000-0002-8271-2284

Notes

The authors declare no competing financial interest.

DOI: 10.1021/acsphotonics.9b00290
ACS Photonics 2019, 6, 1365−1371

■ ACKNOWLEDGMENTS

We thank Wieland Schöllkopf and Sandy Gewinner for operating the FEL. D.S.K. and D.F.S. acknowledge funding support from the Office of Naval Research. J.D.C. acknowledges financial support from the Office of Naval Research under grant N00014-18-2107 and from Vanderbilt School of Engineering. We thank Christopher J. Winta for careful reading of the paper.

■ REFERENCES

(1) Kauranen, M.; Zayats, A. V. Nonlinear plasmonics. *Nat. Photonics* **2012**, *6*, 737−748.
(2) Lu, H.; Liu, X.; Wang, L.; Gong, Y.; Mao, D. Ultrafast all-optical switching in nanoplasmonic waveguide with Kerr nonlinear resonator. *Opt. Express* **2011**, *19*, 2910.
(3) Ren, M.; Jia, B.; Ou, J.-Y.; Plum, E.; Zhang, J.; MacDonald, K. F.; Nikolaenko, A. E.; Xu, J.; Gu, M.; Zheludev, N. I. Nanostructured Plasmonic Medium for Terahertz Bandwidth AllOptical Switching. *Adv. Mater.* **2011**, *23*, 5540−5544.
(4) Sederberg, S.; Elezzabi, A. Y. Coherent Visible-Light-Generation Enhancement in Silicon-Based Nanoplasmonic Waveguides via Third-Harmonic Conversion. *Phys. Rev. Lett.* **2015**, *114*, 227401.
(5) Shibanuma, T.; Grinblat, G.; Albella, P.; Maier, S. A. Efficient Third Harmonic Generation from MetalDielectric Hybrid Nanoantennas. *Nano Lett.* **2017**, *17*, 2647−2651.
(6) Nie, S.; Emory, S. R. Probing Single Molecules and Single Nanoparticles by Surface-Enhanced Raman Scattering. *Science* **1997**, *275*, 1102−1106.
(7) Kneipp, K.; Wang, Y.; Kneipp, H.; Perelman, L. T.; Itzkan, I.; Dasari, R. R.; Feld, M. S. Single Molecule Detection Using Surface-Enhanced Raman Scattering (SERS). *Phys. Rev. Lett.* **1997**, *78*, 1667−1670.
(8) Caldwell, J. D.; Lindsay, L.; Giannini, V.; Vurgaftman, I.; Reinecke, T. L.; Maier, S. A.; Glembocki, O. J. Low-loss, infrared and terahertz nanophotonics using surface phonon polaritons. *Nanophotonics* **2015**, *4*, 44−68.
(9) Hillenbrand, R.; Taubner, T.; Keilmann, F. Phonon-enhanced lightmatter interaction at the nanometre scale. *Nature* **2002**, *418*, 159−162.
(10) Wang, T.; Li, P.; Hauer, B.; Chigrin, D. N.; Taubner, T. Optical Properties of Single Infrared Resonant Circular Microcavities for Surface Phonon Polaritons. *Nano Lett.* **2013**, *13*, 5051−5055.
(11) Caldwell, J. D.; Glembocki, O. J.; Francescato, Y.; Sharac, N.; Giannini, V.; Bezares, F. J.; Long, J. P.; Owrutsky, J. C.; Vurgaftman, I.; Tischler, J. G.; et al. Low-Loss, Extreme Subdiffraction Photon Confinement via Silicon Carbide Localized Surface Phonon Polariton Resonators. *Nano Lett.* **2013**, *13*, 3690−3697.
(12) Autore, M.; Li, P.; Dolado, I.; AlfaroMozaz, F. J.; Esteban, R.; Atxabal, A.; Casanova, F.; Hueso, L. E.; Alonso-González, P.; Aizpurua, J.; et al. Boron nitride nanoresonators for phonon-enhanced molecular vibrational spectroscopy at the strong coupling limit. *Light: Sci. Appl.* **2018**, *7*, 17172.
(13) Chen, Y.; Francescato, Y.; Caldwell, J. D.; Giannini, V.; Maß, T. W. W.; Glembocki, O. J.; Bezares, F. J.; Taubner, T.; Kasica, R.; Hong, M.; et al. Spectral Tuning of Localized Surface Phonon Polariton Resonators for Low-Loss Mid-IR Applications. *ACS Photonics* **2014**, *1*, 718−724.
(14) Caldwell, J. D.; Kretinin, A. V.; Chen, Y.; Giannini, V.; Fogler, M. M.; Francescato, Y.; Ellis, C. T.; Tischler, J. G.; Woods, C. R.; Giles, A. J.; et al. Sub-diffractional volume-confined polaritons in the natural hyperbolic material hexagonal boron nitride. *Nat. Commun.* **2014**, *5*, 5221.
(15) Giles, A. J.; Dai, S.; Vurgaftman, I.; Hoffman, T.; Liu, S.; Lindsay, L.; Ellis, C. T.; Assefa, N.; Chatzakis, I.; Reinecke, T. L.; et al. Ultralow-loss polaritons in isotopically pure boron nitride. *Nat. Mater.* **2018**, *17*, 134−139.
(16) Ferrell, R. A. Predicted Radiation of Plasma Oscillations in Metal Films. *Phys. Rev.* **1958**, *111*, 1214−1222.
(17) Berreman, D. W. Infrared Absorption at Longitudinal Optic Frequency in Cubic Crystal Films. *Phys. Rev.* **1963**, *130*, 2193−2198.
(18) McAlister, A. J.; Stern, E. A. Plasma Resonance Absorption in Thin Metal Films. *Phys. Rev.* **1963**, *132*, 1599−1602.
(19) Bösenberg, J.; Raether, H. PlasmaResonance Emission of Potassium, Excited by Light. *Phys. Rev. Lett.* **1967**, *18*, 397−398.
(20) Burke, J. J.; Stegeman, G. I.; Tamir, T. Surface-polariton-like waves guided by thin, lossy metal films. *Phys. Rev. B: Condens. Matter Mater. Phys.* **1986**, *33*, 5186−5201.
(21) Bichri, A.; Lafait, J.; Welsch, H. Visible and infrared optical properties of Ag/SiO 2 multilayers: radiative virtual modes and coupling effects. *J. Phys.: Condens. Matter* **1993**, *5*, 7361−7374.
(22) Vassant, S.; Hugonin, J.-P.; Marquier, F.; Greffet, J.-J. Berreman mode and epsilon near zero mode. *Opt. Express* **2012**, *20*, 23971.
(23) Newman, W. D.; Cortes, C. L.; Atkinson, J.; Pramanik, S.; Decorby, R. G.; Jacob, Z. Ferrell-berreman modes in plasmonic epsilon-near-zero media. *ACS Photonics* **2015**, *2*, 2−7.
(24) Nordin, L.; Dominguez, O.; Roberts, C. M.; Streyer, W.; Feng, K.; Fang, Z.; Podolskiy, V. A.; Hoffman, A. J.; Wasserman, D. Mid-infrared epsilon-nearzero modes in ultra-thin phononic films. *Appl. Phys. Lett.* **2017**, *111*, No. 091105.
(25) Campione, S.; Brener, I.; Marquier, F. Theory of epsilon-near-zero modes in ultrathin films. *Phys. Rev. B: Condens. Matter Mater. Phys.* **2015**, *91*, 121408.
(26) Shaykhutdinov, T.; Furchner, A.; Rappich, J.; Hinrichs, K. Mid-infrared nanospectroscopy of Berreman mode and epsilon-near-zero local field confinement in thin films. *Opt. Mater. Express* **2017**, *7*, 3706.
(27) Li, Y.; Kita, S.; Muñoz, P.; Reshef, O.; Vulis, D. I.; Yin, M.; Lončar, M.; Mazur, E. On-chip zero-index metamaterials. *Nat. Photonics* **2015**, *9*, 738−742.
(28) Liberal, I.; Engheta, N. Near-zero refractive index photonics. *Nat. Photonics* **2017**, *11*, 149−158.
(29) Joannopoulos, J. D.; Johnson, S. G.; Winn, J. N.; Meade, R. D. *Photonic Crystals: Molding the Flow of Light*; Princeton University Press, 2008.
(30) Burgos, S. P.; de Waele, R.; Polman, A.; Atwater, H. A. A single-layer wide-angle negative-index metamaterial at visible frequencies. *Nat. Mater.* **2010**, *9*, 407−412.
(31) Sakoda, K. *Optical Properties of Photonic Crystals*; Springer Series in Optical Sciences; Springer-Verlag: Berlin/Heidelberg, 2005; Vol. *80*; p 258.
(32) Argyropoulos, C.; D'Aguanno, G.; Alù, A. Giant second-harmonic generation efficiency and ideal phase matching with a double ϵ-near-zero cross-slit metamaterial. *Phys. Rev. B: Condens. Matter Mater. Phys.* **2014**, *89*, 235401.
(33) Vassant, S.; Archambault, A.; Marquier, F.; Pardo, F.; Gennser, U.; Cavanna, A.; Pelouard, J. L.; Greffet, J. J. Epsilon-Near-Zero Mode for Active Optoelectronic Devices. *Phys. Rev. Lett.* **2012**, *109*, 237401.
(34) Vassant, S.; Moldovan Doyen, I.; Marquier, F.; Pardo, F.; Gennser, U.; Cavanna, A.; Pelouard, J. L.; Greffet, J. J. Electrical modulation of emissivity. *Appl. Phys. Lett.* **2013**, *102*, No. 081125.
(35) Vasudev, A. P.; Kang, J.-H.; Park, J.; Liu, X.; Brongersma, M. L. Electro-optical modulation of a silicon waveguide with an epsilon-near-zero material. *Opt. Express* **2013**, *21*, 26387.
(36) Luk, T. S.; Campione, S.; Kim, I.; Feng, S.; Jun, Y. C.; Liu, S.; Wright, J. B.; Brener, I.; Catrysse, P. B.; Fan, S.; et al. Directional perfect absorption using deep subwavelength low-permittivity films. *Phys. Rev. B: Condens. Matter Mater. Phys.* **2014**, *90*, No. 085411.
(37) Feng, S.; Halterman, K. Coherent perfect absorption in epsilon-near-zero metamaterials. *Phys. Rev. B: Condens. Matter Mater. Phys.* **2012**, *86*, 165103.
(38) Berini, P. Plasmon-polariton waves guided by thin lossy metal films of finite width: Bound modes of asymmetric structures. *Phys. Rev. B: Condens. Matter Mater. Phys.* **2001**, *63*, 125417.
(39) Berini, P. Long-range surface plasmon polaritons. *Adv. Opt. Photonics* **2009**, *1*, 484.
(40) Vincenti, M. A.; de Ceglia, D.; Ciattoni, A.; Scalora, M. Singularity-driven second- and third-harmonic generation at ϵ-near-

DOI: 10.1021/acsphotonics.9b00290
ACS Photonics 2019, 6, 1365−1371

zero crossing points. *Phys. Rev. A: At., Mol., Opt. Phys.* **2011**, *84*, No. 063826.
(41) Capretti, A.; Wang, Y.; Engheta, N.; Dal Negro, L. Comparative Study of SecondHarmonic Generation from Epsilon-NearZero Indium Tin Oxide and Titanium Nitride Nanolayers Excited in the NearInfrared Spectral Range. *ACS Photonics* **2015**, *2*, 1584−1591.
(42) Luk, T. S.; de Ceglia, D.; Liu, S.; Keeler, G. A.; Prasankumar, R. P.; Vincenti, M. A.; Scalora, M.; Sinclair, M. B.; Campione, S. Enhanced third harmonic generation from the epsilonnear-zero modes of ultrathin films. *Appl. Phys. Lett.* **2015**, *106*, 151103.
(43) Capretti, A.; Wang, Y.; Engheta, N.; Dal Negro, L. Enhanced third-harmonic generation in Si-compatible epsilon-near-zero indium tin oxide nanolayers. *Opt. Lett.* **2015**, *40*, 1500.
(44) Raether, H. *Surface Plasmons on Smooth and Rough Surfaces and on Gratings*; Springer Tracts in Modern Physics; Springer Berlin Heidelberg: Berlin, Heidelberg, 1988; Vol. *111*.
(45) Archambault, A.; Teperik, T. V.; Marquier, F.; Greffet, J. J. Surface plasmon Fourier optics. *Phys. Rev. B: Condens. Matter Mater. Phys.* **2009**, *79*, 195414.
(46) Alexander, R. W.; Kovener, G. S.; Bell, R. J. Dispersion Curves for Surface Electromagnetic Waves with Damping. *Phys. Rev. Lett.* **1974**, *32*, 154−157.
(47) Kliewer, K. L.; Fuchs, R. Optical Modes of Vibration in an Ionic Crystal Slab Including Retardation. II. Radiative Region. *Phys. Rev.* **1966**, *150*, 573−588.
(48) Paarmann, A.; Razdolski, I.; Melnikov, A.; Gewinner, S.; Schöllkopf, W.; Wolf, M. Second harmonic generation spectroscopy in the Reststrahl band of SiC using an infrared free-electron laser. *Appl. Phys. Lett.* **2015**, *107*, No. 081101.
(49) Schöllkopf, W.; Gewinner, S.; Junkes, H.; Paarmann, A.; von Helden, G.; Bluem, H.; Todd, A. M. M. The new IR and THz FEL facility at the Fritz Haber Institute in Berlin. *Proc. of SPIE*; SPIE, 2015; p 95121L. DOI: 10.1117/12.2182284
(50) Paarmann, A.; Razdolski, I.; Gewinner, S.; Schöllkopf, W.; Wolf, M. Effects of crystal anisotropy on optical phonon resonances in midinfrared second harmonic response of SiC. *Phys. Rev. B: Condens. Matter Mater. Phys.* **2016**, *94*, 134312.
(51) Passler, N. C.; Razdolski, I.; Gewinner, S.; Schöllkopf, W.; Wolf, M.; Paarmann, A. Second-Harmonic Generation from Critically Coupled Surface Phonon Polaritons. *ACS Photonics* **2017**, *4*, 1048−1053.
(52) Shen, Y. Optical Second Harmonic Generation At Interfaces. *Annu. Rev. Phys. Chem.* **1989**, *40*, 327−350.
(53) Passler, N. C.; Paarmann, A. Generalized 4 × 4 matrix formalism for light propagation in anisotropic stratified media: study of surface phonon polaritons in polar dielectric heterostructures. *J. Opt. Soc. Am. B* **2017**, *34*, 2128.
(54) Tairov, Y.; Tsvetkov, V. Progress in controlling the growth of polytypic crystals. *Prog. Cryst. Growth Charact.* **1983**, *7*, 111−162.
(55) Taylor, K. M.; Lenie, C. Some Properties of Aluminum Nitride. *J. Electrochem. Soc.* **1960**, *107*, 308.
(56) Moore, W. J.; Freitas, J. A.; Holm, R. T.; Kovalenkov, O.; Dmitriev, V. Infrared dielectric function of wurtzite aluminum nitride. *Appl. Phys. Lett.* **2005**, *86*, 141912.
(57) Davydov, V. Y.; Kitaev, Y. E.; Goncharuk, I. N.; Smirnov, A. N.; Graul, J.; Semchinova, O.; Uffmann, D.; Smirnov, M. B.; Mirgorodsky, A. P.; Evarestov, R. A. Phonon dispersion and Raman scattering in hexagonal GaN and AlN. *Phys. Rev. B: Condens. Matter Mater. Phys.* **1998**, *58*, 12899−12907.
(58) Alam, M. Z.; De Leon, I.; Boyd, R. W. Large optical nonlinearity of indium tin oxide in its epsilon-near-zero region. *Science* **2016**, *352*, 795−797.
(59) Kinsey, N.; DeVault, C.; Kim, J.; Ferrera, M.; Shalaev, V. M.; Boltasseva, A. Epsilon-near-zero Al-doped ZnO for ultrafast switching at telecom wavelengths. *Optica* **2015**, *2*, 616.
(60) Yang, Y.; Kelley, K.; Sachet, E.; Campione, S.; Luk, T. S.; Maria, J.-P.; Sinclair, M. B.; Brener, I. Femtosecond optical polarization switching using a cadmium oxide-based perfect absorber. *Nat. Photonics* **2017**, *11*, 390−395.
(61) Passler, N. C.; Gubbin, C. R.; Folland, T. G.; Razdolski, I.; Katzer, D. S.; Storm, D. F.; Wolf, M.; De Liberato, S.; Caldwell, J. D.; Paarmann, A. Strong Coupling of Epsilon-Near-Zero Phonon Polaritons in Polar Dielectric Heterostructures. *Nano Lett.* **2018**, *18*, 4285−4292.
(62) Runnerstrom, E. L.; Kelly, K. P.; Folland, T. G.; Engheta, N.; Caldwell, J. D.; Maria, J.-P. Polaritonic hybrid-epsilonnear-zero modes: engineering strong optoelectronic coupling and dispersion in doped cadmium oxide bilayers. *arXiv:1808.03847 [cond-mat.mes-hall]* **2019**, 7.
(63) Lynch, D. W.; Hunter, W. Comments on the Optical Constants of Metals and an Introduction to the Data for Several Metals. *Handbook of Optical Constants of Solids*; Academic Press, 1985; Vol. *1*, pp 275−367.
(64) Rodrigues da Silva, R.; Maĉedo da Silva, R.; Dumelow, T.; da Costa, J. A. P.; Honorato, S. B.; Ayala, A. P. Using Phonon Resonances as a Route to All-Angle Negative Refraction in the FarInfrared Region: The Case of Crystal Quartz. *Phys. Rev. Lett.* **2010**, *105*, 163903.
(65) Yoxall, E.; Schnell, M.; Nikitin, A. Y.; Txoperena, O.; Woessner, A.; Lundeberg, M. B.; Casanova, F.; Hueso, L. E.; Koppens, F. H. L.; Hillenbrand, R. Direct observation of ultraslow hyperbolic polariton propagation with negative phase velocity. *Nat. Photonics* **2015**, *9*, 674−678.
(66) Li, P.; Lewin, M.; Kretinin, A. V.; Caldwell, J. D.; Novoselov, K. S.; Taniguchi, T.; Watanabe, K.; Gaussmann, F.; Taubner, T. Hyperbolic phonon-polaritons in boron nitride for near-field optical imaging and focusing. *Nat. Commun.* **2015**, *6*, 7507.
(67) Dai, S.; Ma, Q.; Andersen, T.; Mcleod, A. S.; Fei, Z.; Liu, M. K.; Wagner, M.; Watanabe, K.; Taniguchi, T.; Thiemens, M.; et al. Subdiffractional focusing and guiding of polaritonic rays in a natural hyperbolic material. *Nat. Commun.* **2015**, *6*, 6963.
(68) Khurgin, J. B. How to deal with the loss in plasmonics and metamaterials. *Nat. Nanotechnol.* **2015**, *10*, 2−6.

DOI: 10.1021/acsphotonics.9b00290
ACS Photonics 2019, 6, 1365−1371